

## Size and Topology Effects on Fracture Behavior of Cellular Structures

Yan Wu, Li Yang

Department of Industrial Engineering, University of Louisville, Louisville, KY 40292

### Abstract

Cellular structures can deform by either the bending, stretching or both of the cell walls or cell struts. In this study, the fracture characteristics of multiple typical cellular structures that represent both the bending-dominated and stretching-dominated structures were investigated. An analytical model based on the matrix displacement method was established for the analysis of the fracture progression of the cellular structures, which was consequently employed for the fracture analysis of the cellular structures under various geometry design conditions including cell topology, cell size and number of unit cells. From the results, it was shown that the fracture propagation patterns and stress characteristics of the two cellular designs (diamond and triangular) exhibit different dependencies on their geometry designs and cellular patterns. While the stretch-dominated triangular structure exhibit higher fracture strength compared to the bending-dominated diamond structure, it also exhibits more rapid fracture propagation and more significant size effect.

### 1. Introduction

Cellular structures are a class of structures with low densities and novel physical, mechanical, thermal, electrical and acoustic properties. In general, these structures offer significant potentials for a broad range of applications such as light weighting, energy absorption, and thermal management. There exist an abundance of literatures have investigated the mechanical properties of various periodic cellular structures such as Poisson's ratio, Young's modulus, ultimate strength and yield strength [1-8]. For the fracture properties of the cellular structures, most of the efforts were focused on the fracture behaviors of infinite cellular structures or cellular structures with a large number of unit cells [9-17]. One of the earlier modeling works of cellular fracture by Ashby investigated the cellular structure subjected to remote stress [9]. Similar to the analysis of the conventional linear elastic fracture mechanics, it was assumed that the critical strut directly ahead of the macroscopic crack tip would fail when its stress level of that strut reached the ultimate material strength [9]. Such approach was also adopted by various other works as it is both mathematically efficient and conceptually convenient. Using this approach, generally unit cell based modeling is used to facilitate the simplification of the analysis. However, the modeling of unit cell structures imposes multiple assumptions that could potentially introduce errors into the designs [18]. For example, in order to ensure that the loading conditions of a single unit cell are representative of the entire structure, it must be assumed that the structure is subjected to remote stresses and that the boundary constraints can be ignored. However, as actual structures always have finite dimensions and therefore deviate from this condition, size effects occur with cellular structures. Both experimental and modeling-based size effect studies have been reported for various cellular structures [19-23]. However, very little is currently available on the effects of size and topology on the fracture pattern of cellular structures.

In this work, attempts were made to model fracture properties of two 2D lattice structures that represent the bending-dominated and stretching-dominated structures. The combined effect of cellular pattern size and topology on the fracture characteristics of the cellular designs were investigated analytically. This paper is organized into four sections. The modeling of the fracture of cellular structures using the matrix displacement method is described in Section 2; next, the geometry selection and creation is introduced in Section 3; finally, the fracture pattern of different structures will be compared and discussed in Section 4.

## **2. Matrix displacement method for fracture properties modeling**

The cellular structures are considered as networks of interconnected struts or walls with porosities. Each strut or wall is considered to be rigidly connected at the nodes. Therefore, without losing generality, a 2D beam problem was considered. For each node, there are three degrees of freedom/displacement, which are axial displacement, vertical displacement and the rotational angle. The respective forces are the axial force, shear force and the moment. Each strut or wall consists of two nodes, which correspond to six degrees of freedom as shown in Fig.1. These six displacements of the two nodes of an element can be described under both the global coordinate system ( $\bar{x}\bar{o}\bar{y}$ ) and local coordinate system ( $xoy$ ). For the local coordinate system, the  $x$  axis is set to be along the axis of the element from node  $i$  to node  $j$ .

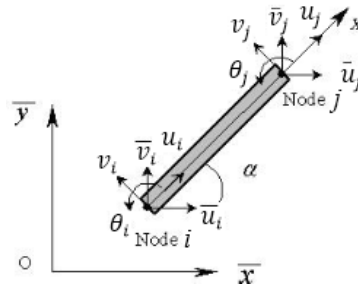


Fig. 1 The global coordinate system ( $\bar{x}\bar{o}\bar{y}$ ) and local coordinate system ( $xoy$ ) of the 2D beam

Under the local coordinate system ( $xoy$ ), the forces at the ends of a beam element are related to the corresponding displacements at the ends by the element stiffness matrix, i.e.,

$$\begin{Bmatrix} F_i^e \\ F_j^e \end{Bmatrix} = [K]^e \begin{Bmatrix} d_i^e \\ d_j^e \end{Bmatrix} \quad (1)$$

where  $d_i^e$  and  $d_j^e$  are the displacement vectors at node  $i$  and  $j$  respectively, and  $F_i^e$  and  $F_j^e$  are force vectors at node  $i$  and  $j$  respectively for the element  $ij$ . Combining the bar stiffness matrix and pure bending beam stiffness matrix, the element stiffness matrix  $[K]^e$  for a six degrees of freedom strut is shown in Eq. (2).  $E$ ,  $A$ ,  $l$  and  $I$  are Young's modulus, area of the cross section, length of the strut and the second moment of inertia, respectively.  $[K]^e$  is only decided by the structure and material and has no dependency on the applied forces.

$$\mathbf{K}^e = \begin{bmatrix} \frac{EA}{l} & 0 & 0 & -\frac{EA}{l} & 0 & 0 \\ 0 & \frac{12EI}{l^3} & \frac{6EI}{l^2} & 0 & -\frac{12EI}{l^3} & \frac{6EI}{l^2} \\ 0 & \frac{6EI}{l^2} & \frac{4EI}{l} & 0 & -\frac{6EI}{l^2} & \frac{2EI}{l} \\ -\frac{EA}{l} & 0 & 0 & \frac{EA}{l} & 0 & 0 \\ 0 & -\frac{12EI}{l^3} & -\frac{6EI}{l^2} & 0 & \frac{12EI}{l^3} & -\frac{6EI}{l^2} \\ 0 & \frac{6EI}{l^2} & \frac{2EI}{l} & 0 & -\frac{6EI}{l^2} & \frac{4EI}{l} \end{bmatrix} \quad (2)$$

Since  $[\mathbf{K}]^e$  is based on the local coordinate system ( $xoy$ ) as shown in Fig.1, and for cellular structures individual struts are likely orientated differently, additional transformation is needed to convert the stiffness matrix into the more consistent global coordinate system ( $\bar{x}\bar{o}\bar{y}$ ). Therefore, the transformation matrix  $[\mathbf{T}]^e$  shown in Eq. (3) was introduced to convert the different local coordinate systems to the global coordinate system.

$$\mathbf{T}_{(6 \times 6)}^e = \begin{bmatrix} \cos \alpha & \sin \alpha & 0 & 0 & 0 & 0 \\ -\sin \alpha & \cos \alpha & 0 & 0 & 0 & 0 \\ 0 & 0 & 1 & 0 & 0 & 0 \\ 0 & 0 & 0 & \cos \alpha & \sin \alpha & 0 \\ 0 & 0 & 0 & -\sin \alpha & \cos \alpha & 0 \\ 0 & 0 & 0 & 0 & 0 & 1 \end{bmatrix} \quad (3)$$

Apply such transformation to the applied forces and the displacements, and the stiffness matrix under global coordinate system  $[\bar{\mathbf{K}}]$  can be expressed

$$[\bar{\mathbf{K}}] = [\mathbf{T}]^{eT} \cdot [\mathbf{K}]^e \cdot [\mathbf{T}]^e. \quad (4)$$

Then one can simply combine all the element stiffness matrices  $[\bar{\mathbf{K}}]$  together to obtain the stiffness matrix for the entire structure. It is noted that the 2D lattice structures are usually subjected to the loading conditions that are applied on the boundaries, and there does not exist external forces at the internal nodes, as shown in Fig. 1. This means that on the boundaries most of the displacements are either zero or known values, and the external forces are always zero at the internal nodes. Therefore, for 2D lattice structures, the displacements  $[\mathbf{d}]$  and forces  $[\mathbf{F}]$  can be divided into the known part and unknown part for further calculation. Therefore, the stiffness matrix Eq. (1) can be rewritten as

$$\begin{bmatrix} A_{11} & A_{12} \\ A_{21} & A_{22} \end{bmatrix} \begin{bmatrix} d_{unknown} \\ d_{known} \end{bmatrix} = \begin{bmatrix} F_{known} \\ F_{unknown} \end{bmatrix} \quad (5)$$

where  $d_{unknown}$  is the vector of unknown displacements,  $d_{known}$  is the vector of known displacements,  $F_{known}$  is a vector of known forces and  $F_{unknown}$  is a vector of unknown forces. From Eq. (5), the unknown displacements can be solved as

$$d_{unknown} = A_{11}^{-1}(F_{known} - A_{12}d_{unknown}). \quad (6)$$

Therefore, with the knowledge of  $d_{known}$ , all the displacement components can be determined for the calculation of the internal forces for each strut. Furthermore, the stress distribution of every strut can be established from the results of the nodal displacements.

To determine the crack propagation pattern of these cellular structures, the principal stresses are used to evaluate the brittle failure of individual struts at each stage of the crack propagation. When the principal stress of one strut or wall reaches the yield strength of the material, it was assumed that the corresponding strut or wall will fracture. The matrix displacement method will be iteratively employed to calculate the stress status of the undamaged part of the structure to determine the sequence of the strut/wall fracture. To better illustrate the idea of the crack propagation of the cellular structures, Fig. 2 shows an example of the crack propagation of a finite honeycomb structure at different stages. The two ends of the honeycomb cellular structures are fixed to rigid platens, which also represents the typical boundary condition of sandwich structures or mechanical testing of cellular cubic samples. For Step 0 shown in Fig. 2, the honeycomb structure exhibits its original shape without any applied displacements. With the increasing of the applied displacement, the honeycomb structure starts to deform. When the applied displacement reaches a critical point, the strut with the maximum principal stress would fail and fracture, as shown in Step 1 in Fig. 2. The red dots shown in Fig.2 identifies the fractured struts, which shows that strut 7-10 fractured at Step 1. As the applied displacement continues to increase, there would be another strut, 2-5, that reaches the critical point and fractures as shown in Step 2. At Step 3 and Step 4, struts 1-3 and 7-11 fractures successively and that the entire structure would fail.

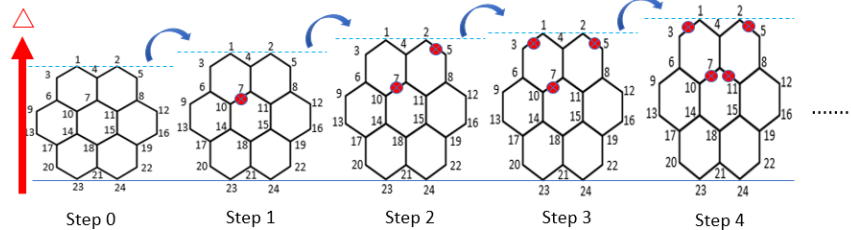


Fig. 2 Stages during fracture

### 3. Geometry design and analysis

2D triangular cellular structure and 2D diamond cellular structure were chosen in this study with their unit cells shown in Fig. 3(b) and (c), which are a typical stretching dominated structure and a bending dominated structure respectively. The design of these cellular structure includes five geometry parameters: the length of each strut ( $L$ ), the opening angle ( $\theta$ ), wall thickness ( $t$ ), number of unit cells ( $N$ ) and the wall width ( $W$ ), as shown in Fig. 3. In this paper, the effect on the fracture properties of the length of each strut ( $L$ ), the opening angle ( $\theta$ ), wall thickness ( $t$ ) and the number of unit cells ( $N$ ) of both types of cellular structures were investigated with a constant boundary wall width of  $W$ .

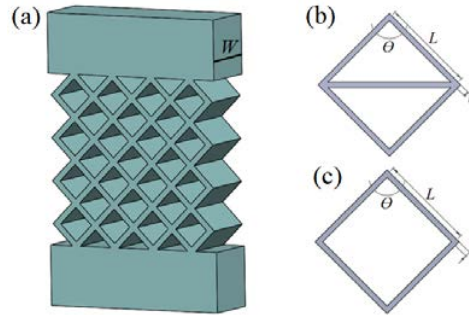


Fig. 3 (a) 3D view of the 2D cellular structure; (b) a triangular unit cell with the essential parameters; (c) a diamond unit cell with the essential parameters

For the wall thickness effect study, five sets of different thicknesses were chosen to evaluate the size effect on the fracture behavior of the 2D diamond structure and 2D triangular structure, which were 0.6, 0.8, 1.0, 1.2 and 1.4mm. In this study, the length of strut was 15mm; the opening angle was  $90^\circ$ ; the number of unit cells in both x and y directions was 4. The original pattern of 2D diamond structure and 2D triangular structure for various wall thicknesses are shown in Fig. 4 and Fig. 5. Variation of the wall thickness has little effect on the whole dimension of these two structures due to the constant strut length. It can be seen that the relative density (SD) is proportional to the wall thickness. The thicker the wall thickness, the more the relative density will be.

For the strut length effect study, five different lengths were investigated, which were 5, 10, 15, 20 and 25mm. In this study, the wall thickness was 1.0mm; the opening angle was  $90^\circ$ ; the number of unit cells in both x and y directions was 4. The original patterns of these cellular structures are presented in Fig. 6 and Fig. 7. The overall length of the structure increases with the increasing strut length. It is obvious that the relative density decreases when the strut length increases.

For the opening angle effect study, five sets of opening angles were investigated, which were  $30^\circ$ ,  $60^\circ$ ,  $90^\circ$ ,  $120^\circ$  and  $150^\circ$ . In this study the wall thickness was 1.0mm; the strut length was 15mm; the number of unit cells in both x and y directions was 4. The original patterns of these cellular structures are presented in Fig. 8 and Fig. 9. For both the 2D diamond structure and 2D triangular structure, the relative density decreases when the opening angle increases from  $30^\circ$  to  $90^\circ$ , while the relative density increases when the opening angle increased from  $90^\circ$  to  $150^\circ$ . However, the relative density shows a symmetric distribution at  $90^\circ$  for the 2D diamond structure.

For the unit cell numbers effect study, five sets of unit cell numbers were investigated, which were 2, 3, 4, 5 and 6. In this study, the wall thickness was 1.0mm; the opening angle was  $90^\circ$ ; the strut length was 15mm. The original patterns of these cellular structures are presented in Fig. 10 and Fig. 11. It is obvious that the overall length of the structure increases with the increasing of the strut length. Besides, the relative density remains the same under different unit cell numbers since the geometry parameters of each unit cells are identical.

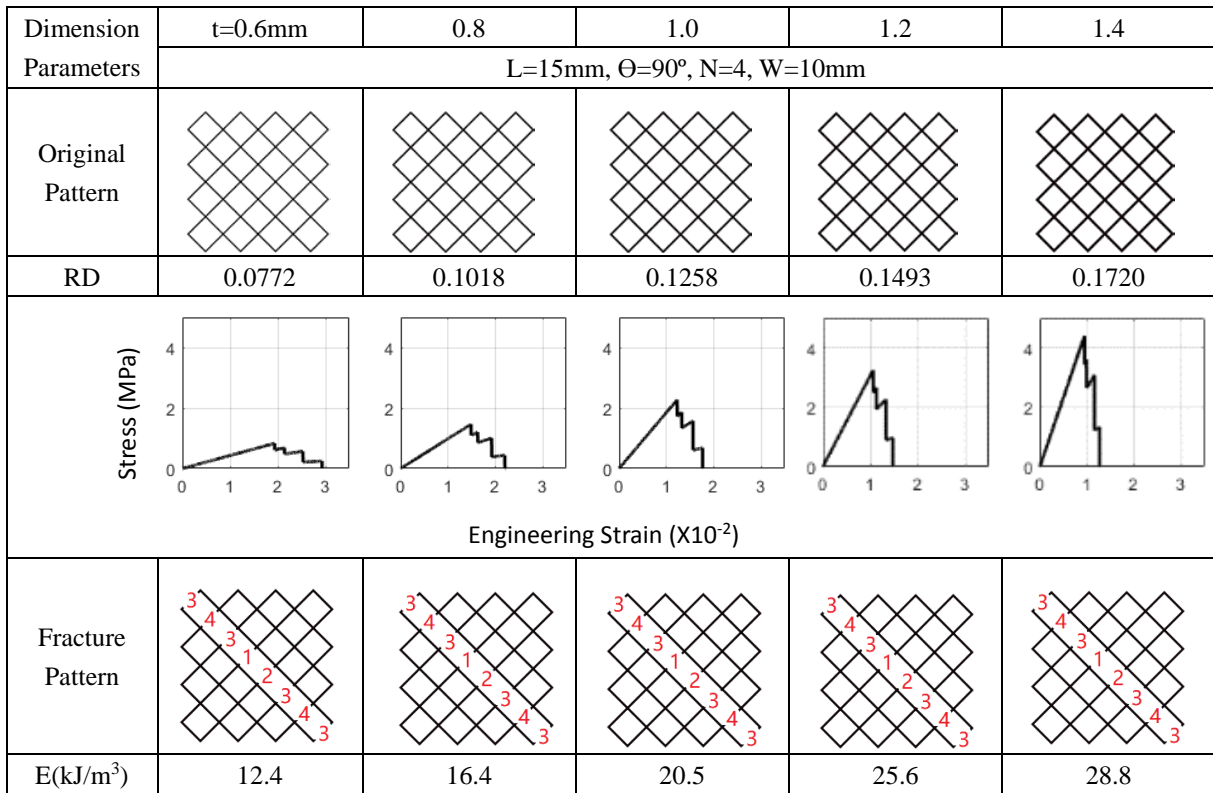


Fig. 4 Effect of wall thickness on the fracture behavior of 2D diamond structure

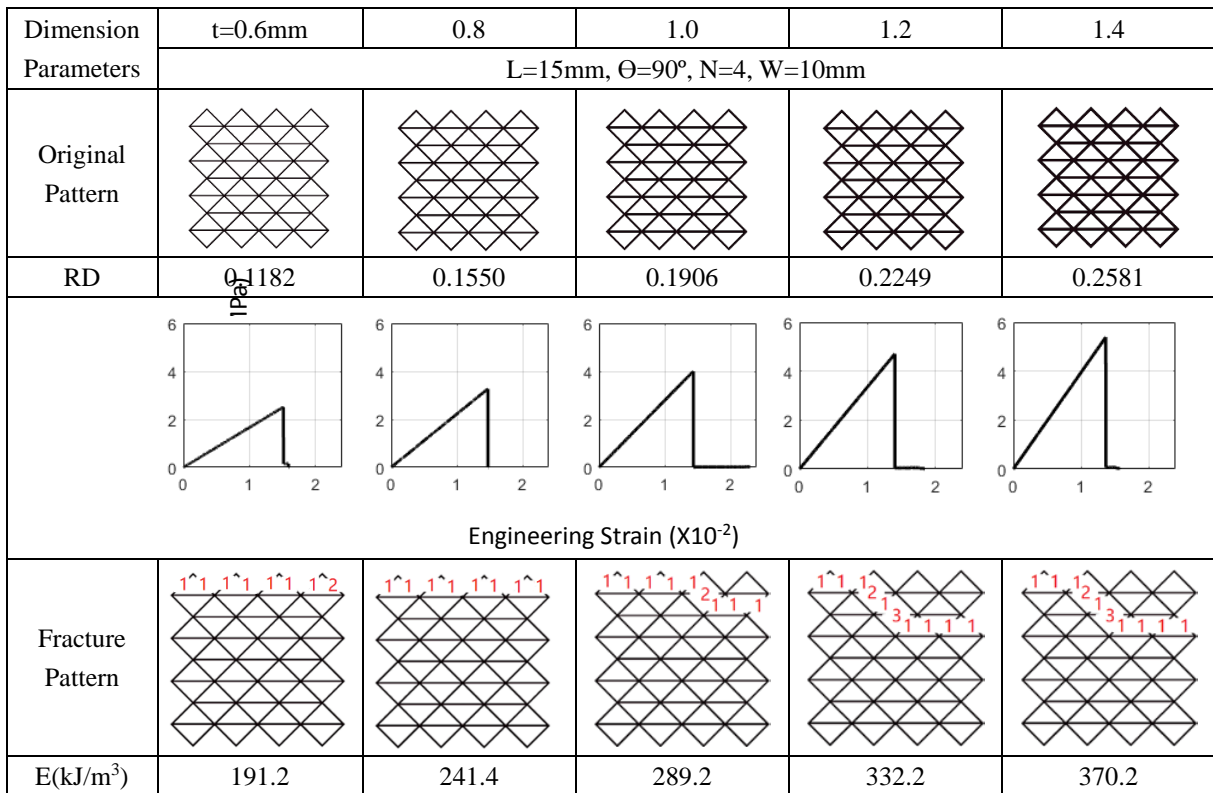


Fig. 5 Effect of wall thickness on the fracture behavior of 2D triangular structure

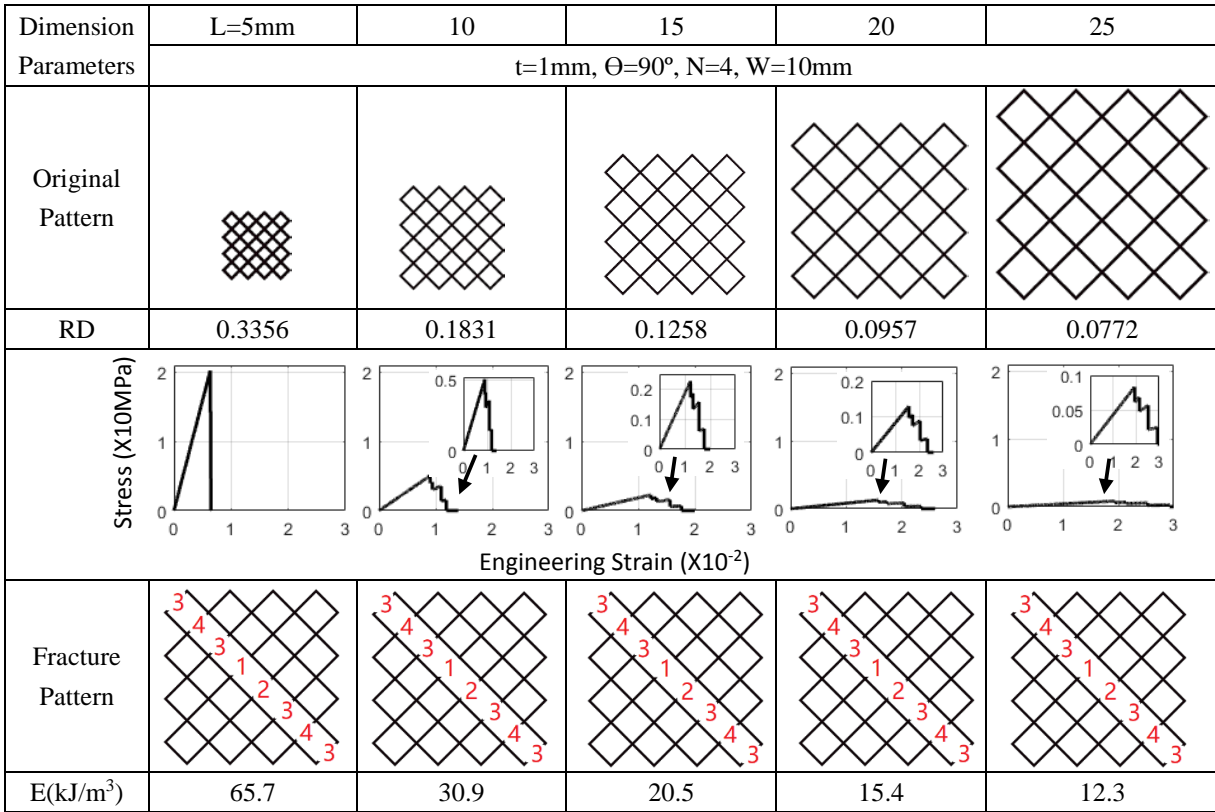


Fig. 6 Effect of strut length on the fracture behavior of 2D diamond structure

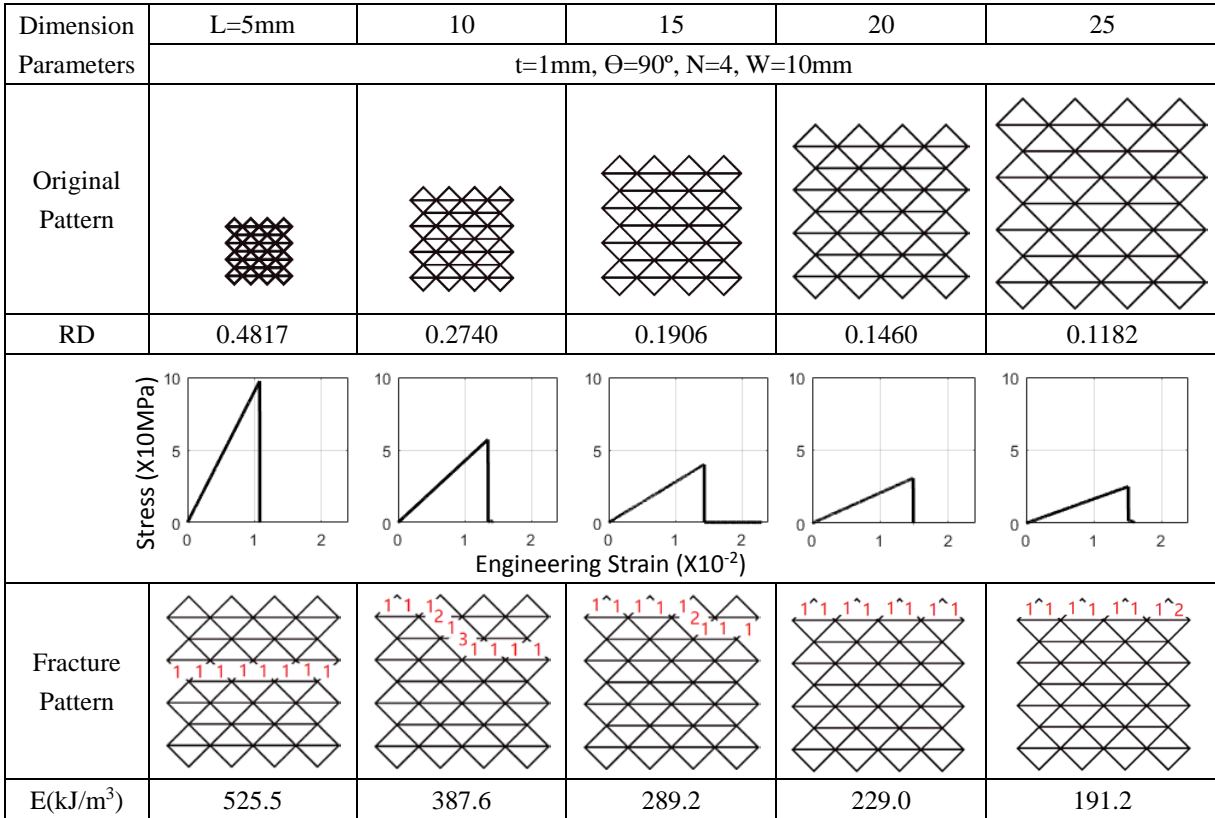


Fig. 7 Effect of strut length on the fracture behavior of 2D triangular structure

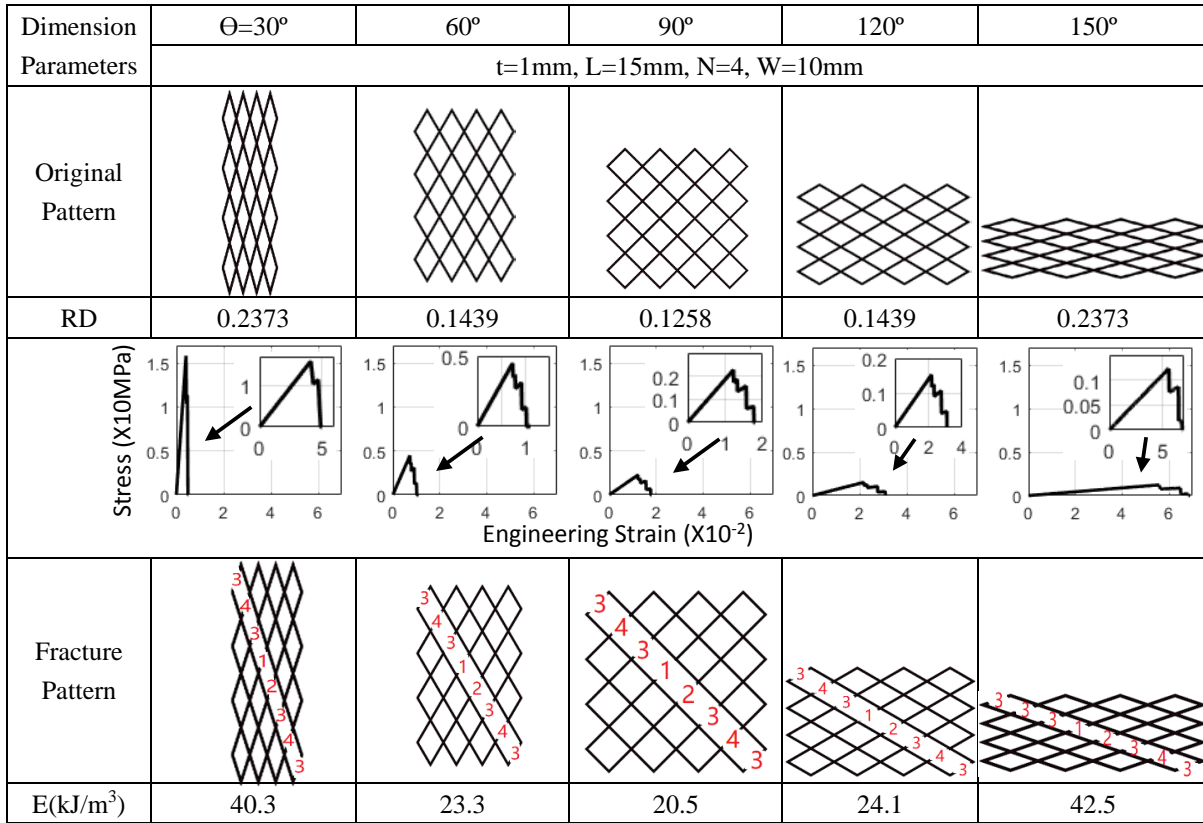


Fig. 8 Effect of opening angle on the fracture behavior of 2D diamond structure

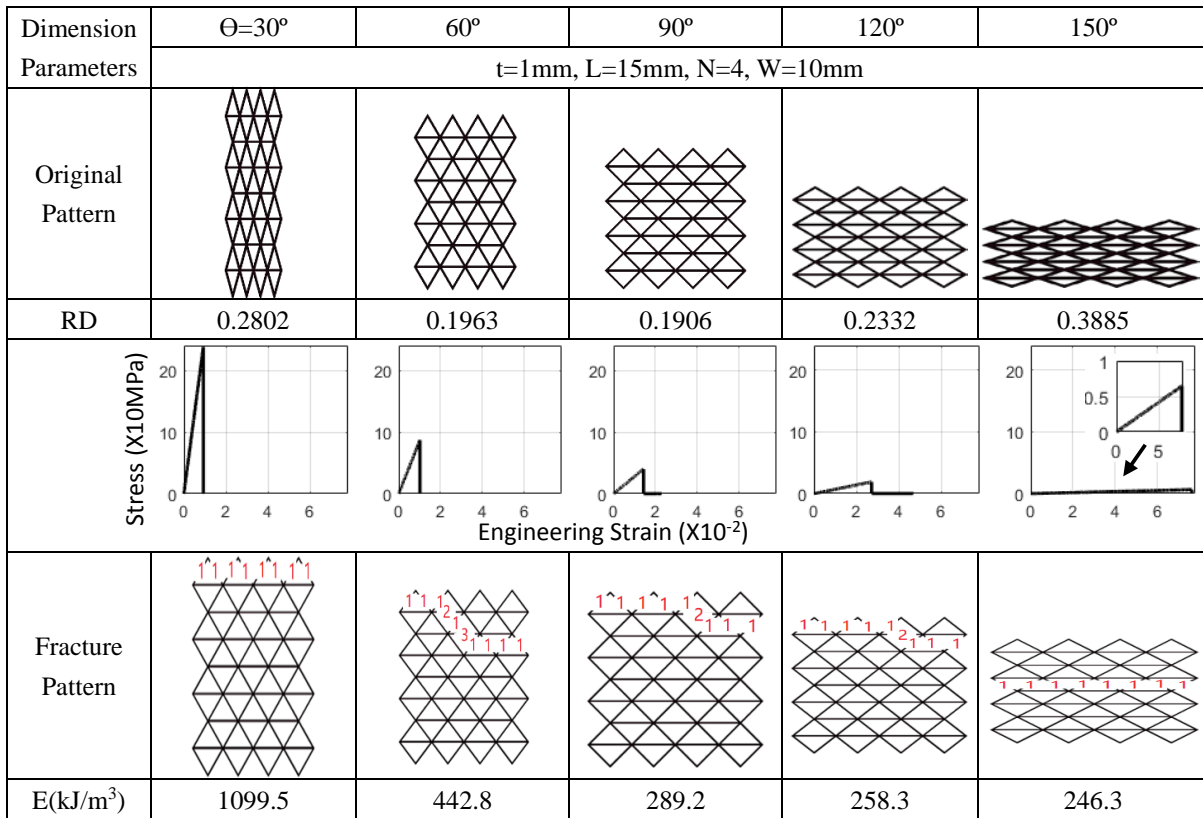


Fig. 9 Effect of opening angle on the fracture behavior of 2D triangular structure

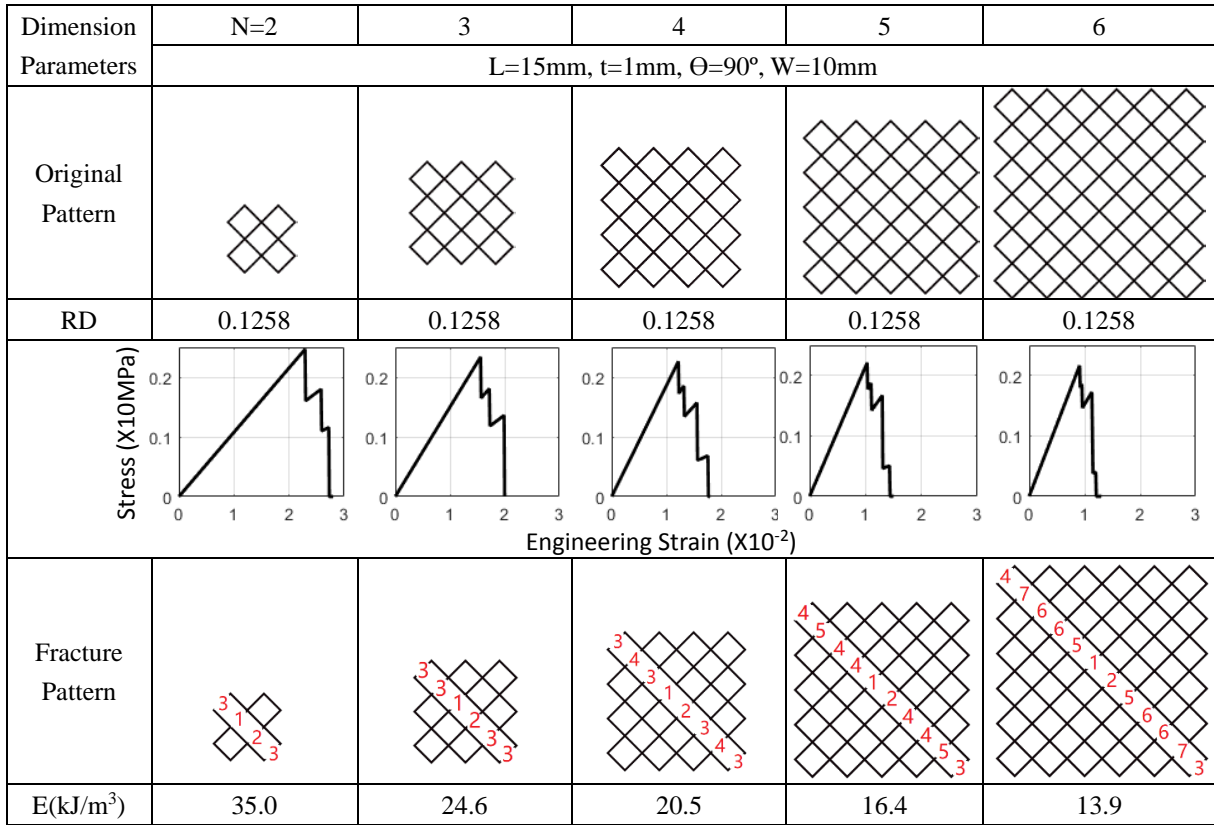


Fig. 10 Effect of unit cell number on the fracture behavior of 2D diamond structure

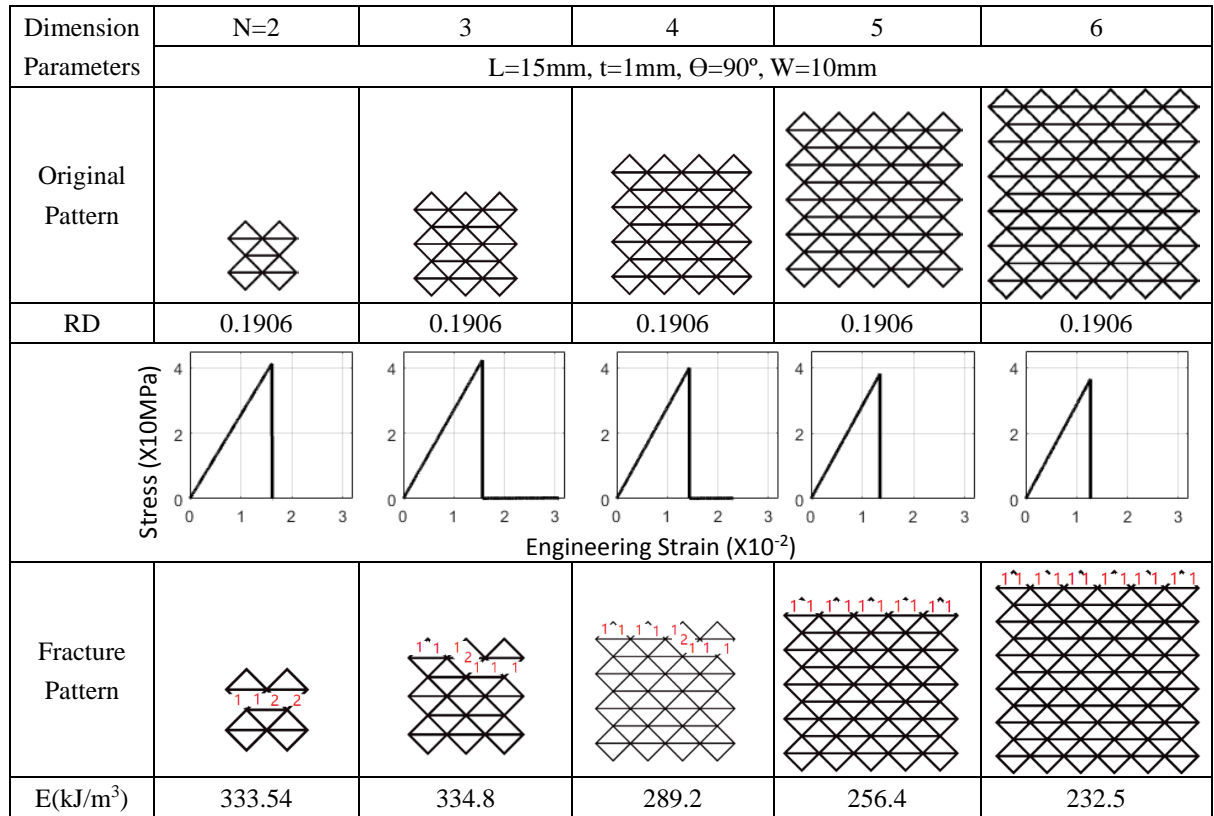


Fig. 11 Effect of unit cell number on the fracture behavior of 2D triangular structure

## **4. Results and discussion**

Fig. 4 to Fig. 11 show the results of the stress-strain curve, the fracture propagation patterns and the energy absorption per volume (E) of the 2D diamond structure and 2D triangular structure with different sets of parameters.

### 4.1 Effect of wall thickness

A comparison of the fracture energy per volume of both 2D diamond structure and 2D triangular structure are shown in Fig. 4 and Fig. 5. The fracture energy per volume of these two structures increases when the wall thickness increases. This implies that the energy absorption capability of these two structures depends highly on the wall thickness. This is because the structures with larger wall thickness have larger stiffness, which can be seen from the stress-strain curve from Fig. 4 and Fig. 5. The maximum strength of the structures at each step of crack propagation increases when the wall thickness increases.

From the stress-strain curves, it is obvious that the bending-dominated diamond structure exhibits sawteeth-like stress fluctuation patterns with multiple stress peaks during the fracture, while the stretching-dominated triangular structure exhibits only one stress peaks. As each peak means that one or more struts fracture, more peaks indicates that the structures exhibit a slow and stable crack growth. Therefore, for the bending-dominated diamond structure, when the applied displacement reaches a critical point, one or multiple struts will fail. After the failure of these struts, the structure can retain its shape if no more displacement is applied. If additional strain is applied, the rest of the structure will continue to deform and absorb more energy before the next strut fractures. The numbers in fracture pattern figure from Fig. 4 show the fracture stages. For example, the number 1 corresponds to the first strut that fractures, and number 2 indicates the next strut to fracture. It was concluded that for the diamond structure, the fracture propagation exhibits more progressive characteristics. On the other hand, the fracture of the stretching-dominated triangular structure appears to be unstable. Once the first strut fractures, large numbers of struts may fracture immediately after the first one, which indicates a possible catastrophic failure of the structures.

For the crack propagation path, the 2D diamond structures show the same diagonal pattern regardless of the wall thickness variations. However, for the 2D triangular structures, the crack propagation exhibits changing patterns when the wall thickness increases from 0.6mm to 1.4mm. When the wall thicknesses is small (0.6mm or 0.8mm), the crack goes through the entire top layer. On the other hand, at higher wall thickness, the crack tends to propagate across multiple layers starting from the top layer.

### 4.2 Effect of strut length

The effect of strut length on the fracture energy per volume of both 2D diamond structure and 2D triangular structure are shown in Fig. 6 and Fig. 7. The fracture energy per volume of these two structures decreases when the strut length increases. This is consistent with the notion

that with decreasing relative density the toughness of the cellular structure decreases. From the stress-strain curves, the bending-dominated diamond structure exhibits multi-stress peak characteristics during the fracture, while the stretching-dominated triangular structure again appears to exhibit only one stress peak. For the crack propagation pattern, the 2D diamond structures again exhibit consistent fracture patterns regardless of the slenderness of the struts, while for the 2D triangular structures, the crack propagation plane exhibits a transition from the middle layers to the boundary layers when strut length increases from 5mm to 25mm.

#### 4.3 Effect of opening angle

The effect of opening angle on the fracture energy per volume of both 2D diamond structure and 2D triangular structure are shown in Fig. 8 and Fig. 9. The energy absorption per volume of the 2D diamond follows the trend of the relative density. When the opening angle varies from  $30^\circ$  to  $90^\circ$ , the energy absorption decreases, while it increases when the opening angle varies from  $90^\circ$  to  $150^\circ$ . However, for the 2D triangular structure, the energy absorption keeps decreasing when the opening angle increases. From the stress-strain curves, the 2D triangular structure exhibits catastrophic fracture while the diamond structure exhibits multi-step crack propagation, which is consistent with the previous observations with the other geometry parameters. The crack propagation of the 2D diamond structures does not appear to be affected by the opening angle. However, for the 2D triangular structures, the crack plane exhibits a transition that starts from the boundary layers and gradually shifts towards the middle layers as the opening angle increases from  $30^\circ$  to  $150^\circ$ .

#### 4.4 Effect of number of unit cells

The effect of cellular pattern size on the fracture energy per volume of both 2D diamond structure and 2D triangular structure are shown in Fig. 10 and Fig. 11. For both types of structures, the fracture energy absorption per volume of these two structures decreases when the unit cell number increases, although the relative densities remain unchanged. This implies that the fracture toughness of the two structures tend to decrease with increasing overall pattern sizes. The 2D diamond structures again exhibit relatively stable fracture crack propagation and insensitivity to geometrical parameters, and the 2D triangular structures exhibit catastrophic crack propagation that follows different patterns when the unit cell number increases.

#### 4.5 Comparison and discussion

For both types of cellular designs, the fracture toughness is strongly dependent on the relative densities, which agrees with the previous conclusions from classic cellular fracture theories. For the 2D bending-dominated diamond structures, the pattern size and other geometry parameters do not have significant influence on its crack propagation characteristic, which always exhibits a diagonal crack path with a relatively slow and stable crack growth. In comparison, The fracture crack propagation characteristics of the 2D stretching-dominated triangular structure appear to be influenced by its geometry designs. Further studies are being carried out to investigate the implications of such observation.

In addition, at same relative density levels, the fracture energy absorption per volume of the 2D triangular structure were significantly higher than that of the 2D diamond structures. The reason for this may be that the strength of the stretching-dominated structures is significantly higher than that of the bending-dominated structures. So even though the bending-dominated structures show a slower crack growth pattern which benefits capacity of energy absorption, the low strength of the structure is hindering its energy absorption performance.

## **5. Conclusions**

In this paper, the fracture properties of the 2D bending-dominated diamond structure and 2D stretching-dominated triangular structures were studied through different designs with varying cell topology, cell size and number of unit cells. The deformation and fracture behavior of these cellular structures was theoretically predicted through an analytical fracture model.

1. The size and topology does not significantly affect the crack propagation patterns of the 2D diamond structures, while they appear to have more significant impact on the crack patterns of the 2D triangular structure.

2. Under the same relative densities, the fracture energy per volume of the 2D stretching-dominated structure were significantly higher than that of the 2D bending-dominated structures.

3. The 2D bending-dominated diamond structure exhibited relatively stable crack propagation pattern, while the 2D stretching-dominated triangular structure appears to exhibit rather catastrophic fracture failure.

## **Acknowledgement**

The authors are grateful of the support from Rapid Prototyping Center (RPC) at University of Louisville. This project was partially supported by the Office of Naval Research (ONR) grant #N00014-16-1-2394.

## **Reference**

- [1] Yan, C., Hao, L., Hussein, A., Young, P., & Raymont, D. (2014). Advanced lightweight 316L stainless steel cellular lattice structures fabricated via selective laser melting. *Materials & Design*, 55, 533-541.
- [2] Smith, M., Guan, Z., & Cantwell, W. J. (2013). Finite element modelling of the compressive response of lattice structures manufactured using the selective laser melting technique. *International Journal of Mechanical Sciences*, 67, 28-41.
- [3] Li, S. J., Murr, L. E., Cheng, X. Y., Zhang, Z. B., Hao, Y. L., Yang, R., ... & Wicker, R. B. (2012). Compression fatigue behavior of Ti-6Al-4V mesh arrays fabricated by electron beam melting. *Acta Materialia*, 60(3), 793-802.
- [4] Deshpande, V. S., Fleck, N. A., & Ashby, M. F. (2001). Effective properties of the octet-truss lattice material. *Journal of the Mechanics and Physics of Solids*, 49(8), 1747-1769.
- [5] Yang, L., Harrysson, O., West, H., & Cormier, D. (2013). Modeling of uniaxial compression in a 3D periodic re-entrant lattice structure. *Journal of Materials Science*, 48(4), 1413-1422.
- [6] Novak, N., Vesenjsek, M., & Ren, Z. (2016). Auxetic Cellular Materials-a Review. *Strojniški vestnik-Journal of Mechanical Engineering*, 62(9), 485-493.
- [7] Maskery, I., Aboulkhair, N. T., Aremu, A. O., Tuck, C. J., Ashcroft, I. A., Wildman, R. D., & Hague, R. J. (2016). A mechanical property evaluation of graded density Al-Si10-Mg lattice structures manufactured by selective laser melting. *Materials Science and Engineering: A*, 670, 264-274.
- [8] Yang, L., Harrysson, O., West, H., & Cormier, D. (2015). Mechanical properties of 3D re-entrant honeycomb auxetic structures realized via additive manufacturing. *International Journal of Solids and Structures*, 69, 475-490.
- [9] Ashby MF (1983) The mechanical properties of cellular solids. *Metall. Trans.* 14(9): 1755-1769.
- [10] Maiti SK, Ashby MF, Gibson LJ (1984) Fracture toughness of brittle cellular solids. *Scripta Metallurgica* 18(3): 213-217.
- [11] O'Masta, M. R., et al. "The fracture toughness of octet-truss lattices." *Journal of the Mechanics and Physics of Solids* 98 (2017): 271-289.
- [12] Alsalla, H., Hao, L., & Smith, C. (2016). Fracture toughness and tensile strength of 316L stainless steel cellular lattice structures manufactured using the selective laser melting technique. *Materials Science and Engineering: A*, 669, 1-6.

- [13] Maimí, P., Turon, A., & Trias, D. (2011). Crack propagation in quasi-brittle two-dimensional isotropic lattices. *Engineering Fracture Mechanics*, 78(1), 60-70.
- [14] Anderson, T.L. (2005). *Fracture mechanics: fundamentals and applications*. CRC Press.
- [15] Griffith, A.A., "The Phenomena of Rupture and Flow in Solids," *Philosophical Transactions, Series A*, Vol. 221, pp. 163-198, 1920.
- [16] Huang, J. S., & Gibson, L. J. (1991). Fracture toughness of brittle honeycombs. *Acta metallurgica et materialia*, 39(7), 1617-1626.
- [17] Huang, J. S., & Gibson, L. J. (1991). Fracture toughness of brittle foams. *Acta metallurgica et materialia*, 39(7), 1627-1636.
- [18] L. Yang, O. Harrysson, D. Cormier, H. West, H. Gong, B. Stucker. Metal cellular structures with additive manufacturing: design and fabrication. *Journal of Materials*.
- [19] J. F. Rakow, A. M. Waas. Size effects and the shear response of aluminum foam. *Mechanics of Materials*. 37(2005): 69-82.
- [20] E. W. Andrews, G. Gioux, P. Onck, L. J. Gibson. Size effects in ductile cellular solids. Part II: experimental results. *International Journal of Mechanical Sciences*. 43(2001): 701-713.2192
- [21] O. Kesler, L. J. Gibson. Size effects in metallic foam core sandwich beams. *Materials Science and Engineering A*. 326(2002): 228-234.
- [22] G. Dai, W. Zhang. Size effects of effective Young's modulus for periodic cellular materials. *Science in China Series G: Physics, Mechanics and Astronomy*. 52(2009), 8: 1262-1270.
- [23] P. R. Onck, E. W. Andrews, L. J. Gibson. Size effects in ductile cellular solids. Part I: modeling. *International Journal of Mechanical Sciences*. 43(2001): 681-699.